Science of the Total Environment 919 (2024) 170559

Contents lists available at ScienceDirect

Science of the Total Environment

journal homepage: www.elsevier.com/locate/scitotenv

Analyzing ozone formation sensitivity in a typical industrial city in China: Implications for effective source control in the chemical transition regime

Yueyuan Niu [a], Yulong Yan [b,c,*], Yiran Xing [a], Xiaolin Duan [a], Ke Yue [b,c], Jiaqi Dong [b,c], Dongmei Hu [a], Yuhang Wang [d], Lin Peng [b,c,*]

[a] MOE Key Laboratory of Resources and Environmental System Optimization, College of Environmental Science and Engineering, North China Electric Power University, Beijing 102206, China
[b] Engineering Research Center of Clean and Low-carbon Technology for Intelligent Transportation, Ministry of Education, School of Environment, Beijing Jiaotong University, Beijing 100044, China
[c] School of Environment, Beijing Jiaotong University, Beijing 100044, China
[d] School of Earth and Atmospheric Sciences, Georgia Institute of Technology, Atlanta, GA 30332, USA

HIGHLIGHTS

- OBM model coupled with the receptor model was used to analyze the source of O_3.
- Vehicle, industry and coal combustion were the main sources of VOCs and NOx.
- The industrial city of Changzhi was in a transition regime of O_3 formation.
- Industrial process was main source of O_3 in industrial cities.
- Ignoring NO_X sensitive might underestimate the anthropogenic source contribution.

GRAPHICAL ABSTRACT

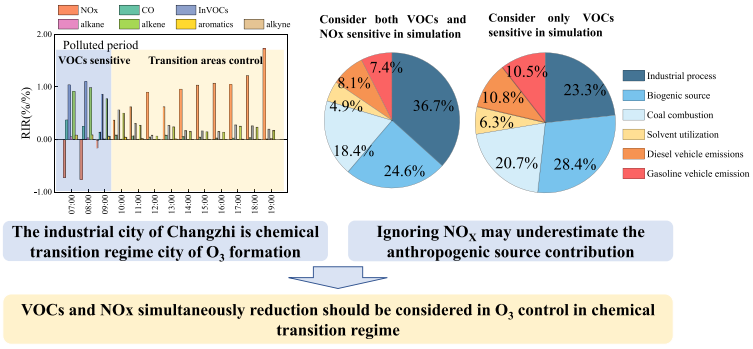

ARTICLE INFO

Editor: Jianmin Chen

Keywords:
O_3 formation sensitivity analysis
Formation mechanism
Source apportionment
Industrial city
Transition regime

ABSTRACT

Volatile organic compounds (VOCs) play a major role in O_3 formation in urban environments. However, the complexity in the emissions of VOCs and nitrogen oxides (NOx) in industrial cities has made it challenging to identify the key factors influencing O_3 formation. This study used observation-based-model (OBM) to analyze O_3 sensitivities to VOCs and NOx during summer in a typical industrial city in China. The OBM model results were coupled with a receptor model to analyze the sources of O_3. Higher concentrations of O_3 precursors were observed during polluted periods indicating that precursor accumulation contributed to the higher maxima of the net ozone formation rate and HOx concentrations. Analyses of ROx· budgets and relative incremental reactivity (RIR) indicated that O_3 production is in a chemical transition regime and was sensitive to both VOCs and NOx. Results from Positive Matrix Factorization (PMF) analysis indicated that gasoline vehicle emissions, industrial processes, and coal combustion were major sources of O_3 precursors. The sensitivities of O_3 production to these sources depend on if both VOC and NOx sensitivities are considered. If only VOCs sensitivity is considered, in

* Corresponding authors at: Engineering Research Center of Clean and Low-carbon Technology for Intelligent Transportation, Ministry of Education, School of Environment, Beijing Jiaotong University, Beijing 100044, China.
E-mail addresses: yanyulong@bjtu.edu.cn (Y. Yan), penglin6611@163.com (L. Peng).

https://doi.org/10.1016/j.scitotenv.2024.170559
Received 2 December 2023; Received in revised form 5 January 2024; Accepted 27 January 2024
Available online 7 February 2024

contrast, the contribution of anthropogenic sources to O_3 production was significantly underestimated. This study highlights the importance of accounting for both VOCs and NOx sensitivities when O_3 chemistry is in a transition regime in O_3 production attribution studies.

1. Introduction

In recent years, tropospheric ozone (O_3) has become an important atmospheric pollutant that is harmful to human health (Cohen et al., 2017). In 168 cities at or above the prefecture level in China, the average concentration of O_3 was 150 μg•m^{-3} in 2021, and the number of days when O_3 is the primary pollutant exceeding the standard accounts for 41.6 % of the total (MEP, 2022). According to the spatial distribution characteristics of O_3 concentrations, Beijing-Tianjin-Hebei and its surrounding areas ("2 + 26" cities) had higher O_3 concentrations (171 μg•m^{-3}) than the Fen-Wei Plain (164 μg•m^{-3}), Yangtze River Delta (151 μg•m^{-3}), Pearl River Delta (153 μg•m^{-3}) and other key areas (MEP, 2022). "2 + 26" cities had developed industries, with coking, steel, cement and other heavy industries, and research on O_3 pollution has been carried out continuously in this region (Duan et al., 2021; Li et al., 2019; Niu et al., 2022; Tan et al., 2022; Ding et al., 2023). However, the phenomenon of elevated O_3 is still widespread, and relevant research should be further promoted according to the industrial characteristics of this region.

O_3 is a typical secondary pollutant that is produced by a series of chemical reactions of precursors such as nitrogen oxides (NOx) and volatile organic compounds (VOCs) under light conditions (Lu et al., 2010; Xu et al., 2017; Zheng et al., 2023). The previous results showed that most urban areas are affected by VOCs, and VOCs play a major role in the production of O_3 (Fan et al., 2021; Mozaffar et al., 2021; Wang et al., 2023; Zhang et al., 2022). However, the emission of precursors in industrial cities is large and complex, and the relationship between O_3 and its precursors is not clear, leading to uncertainty in the main influencing factors of O_3 pollution. The results of a study estimating the VOC emission inventory of China's industrial sources showed that the total industrial VOC emissions peaked in 2016 (16.4 Tg) (Simayi et al., 2022). Although it declined in 2019, it was still 7.7 % higher than that in 2013, and the industries that contributed more to VOCs were the chemical industry, petrochemical industry, coking and other heavy industries (Simayi et al., 2022). For NOx, due to the implementation of ultralow emission transformation measures in recent years in China, NO_2 concentrations decreased in some key industrial areas, but the decrease in NO_2 concentrations also led to the rise in O_3 in some cities due to the complex nonlinear relationship between O_3 and different precursors (Guo et al., 2022; Li et al., 2021; Wang et al., 2022; Wang et al., 2022a). In addition to vehicles and coal combustion emissions, heavy industry, represented by coking, steel, cement and other industries, also emits large amounts of NOx (Cao et al., 2022; Liu et al., 2018). Therefore, it is of great significance to clarify the relationship between O_3 and its precursors in industrial cities for O_3 control in other areas with large and complex precursor emissions.

Hydroxyl radicals (OH·), hydroperoxyl radicals (HO_2·), organic peroxyl radicals (RO_2·) and alkoxyl radicals (RO·), collectively known as ROx·, dominate the oxidative capacity of the atmosphere and influence the formation of O_3 (Zhang et al., 2021). The observation-based 0-D photochemical box model (OBM) is a common model to simulate the photochemical process of O_3 formation and radical recycling, which uses the observation data as constraints, thus avoiding the potential uncertainties in the emission inventory (Ma et al., 2022; Ninneman and Jaffe, 2021; Xuan et al., 2023; Zheng et al., 2023; Sommariva et al., 2020). In addition, the OBM model was also used to assess the sensitivity of O_3 to precursor or source changes through the relative incremental reactivity (RIR) method (Jia et al., 2023; Li et al., 2021; Tan et al., 2019; Zhu et al., 2020). Based on the RIR method, some researchers combined the OBM model and positive matrix factorization (PMF) model to analyze the source of O_3, and the results were more practical than those of the traditional Maximum Incremental Reactivity (MIR) method (Li et al., 2021; Wu and Xie, 2017). Due to the different industrial and economic structures, there are certain differences in the sensitivity of O_3 formation to precursors in different regions. Overall, O_3 formation is more sensitive to VOCs in megacities. For example, the study in Beijing showed that O_3 formation was sensitive to VOCs, while the sensitivity to NOx was negative (Han et al., 2023). And the sensitivity of O_3 formation has shown the same results in megacities such as Shanghai and the Pearl River Delta (Lu et al., 2023a, 2023b; Zhao et al., 2022). Industrial cities have large and complex O_3 precursor emissions, resulting in serious O_3 pollution. There is a lack of research on the sensitivity of high emission precursors to O_3 formation in industrial cities, and there also has a few study on the sources analyze of O_3 based on sensitive precursors in industrial cities during summer.

The above analysis results indicated that it is necessary to focus on industrial cities to study the O_3 source and the influence of precursors on O_3 generation from the perspective of the mechanism, which will provide a basis for clarifying the causes of O_3 pollution in other cities with large and complex precursor emissions. In this study, Changzhi was selected as a typical industrial city to analyze the causes of O_3 pollution and the characteristics of atmospheric photochemical reactions in industrial cities. Changzhi has developed heavy industries such as the chemical industry (coal chemical, petrochemical, etc.), steel industry, coking industry and cement industry, and the production of steel and coke in Changzhi was 6.1 million tons and 15.9 million tons in 2021, respectively, which is higher than other cities in Shanxi Province (SBS, 2022). In this study, an OBM model was used to analyze the characteristics of free radicals, evaluate the process of O_3 generation and the reaction process of atmospheric free radicals, and analyze the sensitive components of O_3 generation in industrial cities. Considering the sensitivity of O_3 to both VOCs and NOx, the OBM model coupled with the PMF model was used to analyze the source of O_3. The aim of this study was to provide guidance for the local government of similarly traditional industrial cities to make strategic decisions on O_3 and its precursors in summertime.

2. Method

2.1. Study sites and measurements

Persistent field measurements were conducted in the typical industrial city - Changzhi from June 2 to June 30, 2021 (Fig. S1). The sampling site was located on the rooftop of the Environmental Monitoring Station of Changzhi, representing an urban environment without nearby large industrial pollution sources, adjacent to the main traffic lanes and surrounded by residential areas. Hourly data of trace gases (O_3, NO, NO_2 and CO) and meteorological parameters (temperature, relative humidity, atmospheric pressure and so on) were obtained from the Environmental Monitoring Station of Changzhi.

An online gas chromatograph–mass selective detector/flame ionization detector (GC–MSD/FID, EXPEC 2000, Puyu Technology Development Co., LTD., Hangzhou) with dual capture and dual separation was used to measure 57 VOCs species with 1-h time resolution, including 29 alkanes, 11 alkenes, 16 aromatics and acetylene. The ambient air was collected in the sampling system into two channels. The samples of both channels were dehydrated and enriched by the cryogenic pretreatment system and then sent to the chromatographic column for separation by direct heat high-temperature thermal desorption. The separated VOCs components were detected by MS and FID detectors, and the qualitative

and quantitative analysis results were obtained through data processing. The detection limit of C2-C5 low carbon alkane is 0.02–0.09 ppbv, propane ≤0.01 ppbv, butene ≤0.05 ppbv, other ≤0.1 ppbv, and the VOCs of C6-C12 detection limit is 0.003–0.019 ppbv. Detailed information on quality assurance and control (QA/QC) can be found in Wang et al. (2021).

2.2. Calculation of the initial concentration of VOCs

As one of the important precursors of O_3 generation, most VOCs have relatively enhanced chemical reactivity. VOCs in ambient air are usually collected and have the characteristics of fresh emission and mixing after oxidation reactions (Li et al., 2021). The research results of VOC observation data directly used for component characteristics and source analysis will differ from the actual situation. Therefore, calculating the initial concentration of VOCs can improve the accuracy of research work, which includes O_3 source apportionment, sensitivity analysis of O_3 formation, simulation of formation mechanism of O_3 and free radical, etc. The dominant chemical reactions of VOCs in the troposphere are OH radical reactions during the daytime, and other removal paths, including deposition and reaction with NO_3 radicals, are assumed to be negligible (Atkinson and Arey, 2003). The InVOCs were calculated using the following equation (Yuan et al., 2013):

$$[VOC_i]_{In} = [VOC_i]_M \times exp(k_i[OH]\Delta t) \quad (1)$$

where $[VOC_i]_{In}$ denotes the initial concentrations of VOCs (InVOCs) species i (ppbv); $[VOC_i]_M$ is the concentrations of measured VOCs (MVOCs) species i (ppbv); k_i represents the rate constant of the reaction between species i and OH radicals ($cm^3 \cdot molecule^{-1} \cdot s^{-1}$) and is estimated based on Eqs. (2)–(3); $[OH]$ is the concentration of OH radicals ($molecule \cdot cm^{-3}$); and Δt is the photochemical consumption time of VOC species i reacting with OH radicals from sources to the receptor (s). The estimation methods of [OH] and Δt are shown in Text S1.

$$k_{OH} = AT^n e^{-B/T} \quad (2)$$

$$k_{OH} = Ae^{-B/T} \quad (3)$$

where A is the Arrhenius constant ($cm^3 \cdot molecule^{-1} \cdot s^{-1}$); B is the ratio of the apparent activation energy (Ea) to the molar gas constant (R) (K); and n is a coefficient, generally $n = 210$. For alkanes, the recommended temperature-dependent expression is a three-parameter expression (Eq. (2)), while for alkenes, alkynes, and aromatics, Eq. (3) is used (Atkinson, 2003). The values of A, B, n, and k_{OH} refer to the study Wang et al., 2022b.

2.3. Model description

2.3.1. Photochemistry model description

Framework for 0-D Atmospheric Modeling (F0AM), an open source zero-dimensional (0-D) atmospheric chemical box model specifically, was designed for use with Master Chemical Mechanism (MCM) (http://mcm.york.ac.uk/MCM/) (Wolfe et al., 2016), and the method has been widely utilized in many studies (Li et al., 2021; Wang et al., 2022b; Zhang et al., 2022; Zheng et al., 2023). More than 5800 chemical species and 17,000 reactions are included in the MCM mechanism. Photolysis frequencies (JO^1D (J1), JNO_2 (J4)) were derived from the NCAR's Tropospheric Ultraviolet and Visible radiation model (TUV v5.3, available at http://cprm.acom.ucar.edu/Models/TUV/Interactive_TUV/), and the other parameters relevant to this study (O_3 column, surface albedo, cloud optical depth, aerosol optical depth, and single scattering albedo) were obtained from https://worldview.earthdata.nasa.gov/ (Li et al., 2021; Wolfe et al., 2016). Dilution mixing was considered, but vertical or horizontal transport of air masses was not involved in this study. The observed meteorological parameters (T, RH, P) and trace gases (NO, NO_2, CO and VOCs) with a time resolution of 1 h were used to constrain the model. The model was run with 00:00 local time (LT) as the initial time. Before simulation, the model was run two days in advance to stabilize the unmeasured species (e.g., radicals).

2.3.2. Source apportionment of VOCs

PMF has been identified as an important receptor model based on the observation data of pollutants, which has been identified as an important method for extracting VOCs sources (Hui et al., 2018; Gao et al., 2020). More details of the model can be found in the user guide (Norris et al., 2014). In this study, PMF was applied to quantitatively analyze the sources of VOCs in Changzhi. The calculation theory of PMF is shown in Eq. (4). The uncertainty of the sample data was calculated using Eq. (5).

$$C_{ik} = \sum_{j=1}^{p} A_{ij}B_{jk} + \varepsilon_{ik}(i = 1, 2, \cdots, n) \quad (4)$$

where C_{ik} represents the concentration of species i in sample k; j and p represent the pollution source j and the number of pollution sources; A_{ij} and B_{jk} represent the source profile and source contribution, respectively; and ε_{ik} represents the residue factor.

$$U = \begin{cases} \sqrt{(E \bullet c)^2 + M^2} & (c > M) \\ \dfrac{5}{6}M & (c \le M) \end{cases} \quad (5)$$

where c was the concentration of species. E was the error ratio (0.2). M was the detection limit of the species.

In this model, the objective function Q is solved with an iterative minimization algorithm, and the Q value must be as small as possible. The objective function was defined in Eq. (6).

$$Q = \sum_{i}^{m} \sum_{k}^{n} \left(\frac{\varepsilon_{ik}}{\sigma_{ik}}\right)^2 \quad (6)$$

where σ_{ik} represents the uncertainty bias of the sample. m and n represent the number of species and the number of samples, respectively.

2.3.3. O_3 production simulation

The ozone production rate (P (O_3)) can be quantified by the oxidation rate of NO to NO_2 by peroxyl radicals (Ma et al., 2022), as expressed in Eq. (7).

$$P(O_3) = k_{HO_2+NO}[HO_2][NO] + k_{RO_2+NO}[RO_2][NO] \quad (7)$$

where $[HO_2]$ and $[RO_2]$ are the concentrations of HO_2 and RO_2 radicals, respectively. k_{HO_2+NO} is the reaction rate between HO_2 radicals and NO. k_{RO_2+NO} is the reaction rate between RO_2 radicals and NO.

Once ozone forms, it will be consumed by OH, HO_2 and alkenes. Additionally, some NO_2 can react with OH, resulting in the formation of nitrate before photolysis (Ma et al., 2022). Additionally, O_3 through photolysis is also considered an important loss path of O_3 (Wang et al., 2022a). The chemical loss is shown in Eq. (8).

$$\begin{aligned} L(O_3) = {} & k_{O_3+OH}[O_3][OH] + k_{O_3+HO_2}[O_3][HO_2] + k_{O_3+alkenes}[O_3][alkenes] \\ & + k_{NO_2+OH}[NO_2][OH] + k_{O(^1D)+H_2O}[O^1D][H_2O] \end{aligned} \quad (8)$$

where $L(O_3)$ is the O_3 chemical loss rate; [OH] is the number concentration of OH radicals; and k_{O_3+OH}, $k_{O_3+HO_2}$, $k_{O_3+alkenes}$, k_{NO_2+OH} and $k_{O(^1D)+H_2O}$ are the reaction rates.

$$Net(O_3) = P(O_3) - L(O_3) \quad (9)$$

Finally, $Net(O_3)$is the net ozone formation rate calculated by the difference between $P(O_3)$ and $L(O_3)$, as expressed in Eq. (9).

The F0AM-MCM model can calculate the RIR, which is defined as the ratio of the decrease in $P(O_3)$ to the decrease in precursor concentra-

tions, to assess the sensitivity of O_3 photochemical production in an area (Cardelino and Chameides, 1995). The calculation equations of RIR and average RIR are shown in Eq. (10) and Eq. (11), respectively (Zeng et al., 2018).

$$RIR = \frac{Net(X) - Net(X - \Delta X)/Net(X)}{\Delta S(X)/S(X)} \quad (10)$$

$$\overline{RIR} = \frac{\sum_1^n [RIR(X) \times Net(O_3)]}{\sum_1^n Net(O_3)} \quad (11)$$

where $Net(X)$ represents the net production rate of a specific species X, Group X, or source X. $Net(X - \Delta X)$ refers to the net production rate of X caused by the hypothetical emission change ΔX. $S(X)$ is the total observed mixing ratio of precursor X. $\Delta S(X)$ is the total mixing ratio change of precursor X caused by the hypothetical emission change (assumed to be 20 % in this study).

The contribution of the VOCs to O_3 formation is calculated by Eq. (12).

$$Contribution(X) = \frac{\overline{RIR}(X) \times con(X)}{\sum_1^m [\overline{RIR}(X) \times con(X)]} \quad (12)$$

where $con(X)$ is the average concentration of source X derived from PMF. m is the number of VOCs groups or sources resolved by PMF.

3. Results and discussion

3.1. Overview characteristics

3.1.1. Initial VOCs concentrations

During the study period, the MVOCs concentrations ranged from 3.6 ppbv to 34.7 ppbv, with a mean value of 12.6 ± 4.8 ppbv. The InVOCs concentrations ranged from 4.5 ppbv to 35.5 ppbv, with a mean value of 14.9 ± 5.3 ppbv. However, the diurnal variation in InVOCs showed a different diurnal curve compared with the MVOCs concentrations, especially during the periods of high light (13 o'clock – 16 o'clock) (Fig. 1). During the daytime (7 o'clock-19 o'clock), the average InVOCs concentration was 16.0 ± 5.8 ppbv, which was 31.1 % higher than the average MVOCs concentration (12.2 ± 4.7 ppbv). VOCs tend to be consumed by photochemical reactions under daytime light, resulting in an underestimate of the actual observed VOCs concentrations, especially in the afternoon (Ma et al., 2022; Wang et al., 2022b). For VOC species, the initial concentrations of alkane, A-alkene (anthropogenic alkene), isoprene, aromatic and alkyne in daytime were 7.2 ppbv, 2.9 ppbv, 2.5 ppbv, 1.5 ppbv and 2.0 ppbv, which were 3.5 %, 76.2 %, 428.7 %, 19.0 % and 1.7 % higher than the measured concentrations, respectively. Alkenes were largely underestimated among the observed VOC species, which play an important role in photochemical reaction processes. Therefore, InVOCs were chosen to study the atmospheric photochemical reaction process in this study.

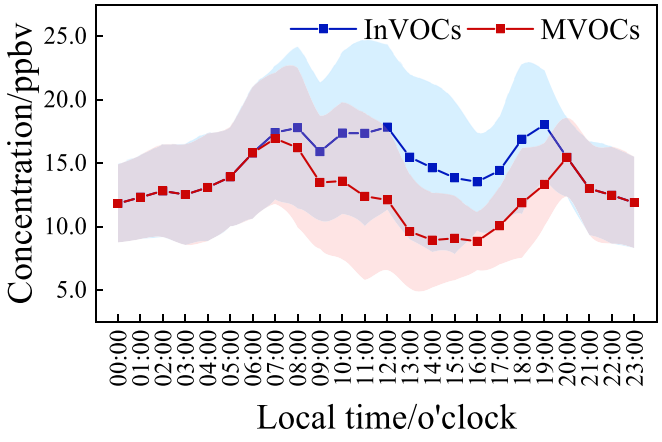

Fig. 1. Diurnal variations in concentrations of InVOCs and MVOCs.

3.1.2. Diurnal variation characteristics of pollutants

The average concentrations and diurnal variation characteristics of atmospheric pollutants (O_3, InVOCs, CO and NO_2) from June 2 to June 30, 2021, were analyzed in this study (Fig. 2). The whole observation period can be classified into two comparable periods: a polluted period (with daily O_3—8H concentrations ≥160 μg•m^{-3}) and a clean period (with daily O_3—8H concentrations <160 μg•m^{-3}). There were 17 polluted days and 12 clean days during the whole observation period. The average hourly concentrations of O_3 were 134 ± 44 μg•m^{-3} during the polluted period, approximately 40.9 % higher than that during the clean period (95 ± 37 μg•m^{-3}). As important precursors of O_3, the average concentrations of InVOCs, CO and NO_2 were 15.5 ± 6.6 ppbv, 1.0 ± 0.4 mg•m^{-3} and 16 ± 11 μg•m^{-3} during the polluted period, which were 23.5 %, 7.1 % and 33.1 % higher than those during the clean period, respectively.

As shown in Fig. 2, O_3 showed a single peak diurnal variation, and the maximum hourly concentrations of O_3 during the polluted period (179 μg•m^{-3}) were 49.2 % higher than those during the clean period (120 μg•m^{-3}). The diurnal variation trends of the three O_3 precursors (InVOCs, NOx and CO) were generally consistent, showing bimodal variation characteristics and reaching their first peak at 8 am. The first peak concentrations of InVOCs, NOx and CO in the morning reached 20.2 ppbv, 34 μg•m^{-3} and 1.4 mg•m^{-3} during the pollution period, respectively. Additionally, the concentrations of InVOCs, NOx and CO in the morning (8:00–13:00) were 35.1 %, 47.3 % and 18.7 % higher during the polluted period than during the clean period, respectively. This phenomenon reflected that the accumulation of precursors in the morning may undergo strong photochemical reactions and be consumed especially in afternoon (13:00–16:00), resulting in O_3 pollution. As showed in Fig. 1, the difference value between InVOCs and MVOCs was higher during 13 o'clock – 16 o'clock, and also indicated the strong photochemical reactions in afternoon. Especially, isoprene had the largest different value between InVOCs and MVOCs, which reached the peak value at 13 o'clock due to the active photochemical reactions. As a secondary pollutant, O_3 is mainly formed by atmospheric photochemical reactions (Lu et al., 2010), and the precursors participate in atmospheric photochemical reactions through reactions with atmospheric oxidants such as OH·, nitrate radicals (NO_3), chlorine atoms, and O_3 (Wang et al., 2017; Xu et al., 2017).

Some research showed that the sources of CO were mainly from coal combustion and industrial process sources, which can be used to reflect the industrial emission level of the city (Cao et al., 2022; Liu et al., 2018). The average concentrations of CO in Changzhi (1.1 mg•m^{-3}) were 37.5 % higher than the average level in China (0.8 mg•m^{-3}) in June 2021, which reflected the higher emission level of precursors in industrial cities (CNEMC, 2023). Thus, to mitigate O_3 pollution in industrial cities, the emission of its precursors should be controlled, and the control of periods at night and morning should not be ignored.

3.2. Mechanism of atmospheric photochemical reaction

3.2.1. O_3 and free radical budget analysis

To demonstrate the accuracy of the model simulation, Fig. S2 analyzed the relationship between the observed O_3 concentration and the simulation O_3 concentration. And there was a significant correlation between observed and simulated O_3 concentration with a squared correlation coefficient of 0.916. To study the atmospheric photochemical reaction mechanism during different periods, the production and loss pathways of O_3 were analyzed in this study (Fig. 3). The maximum net (O_3) during the polluted period was 19.6 ppbv/h, which was 38.2 % higher than that during the clean period (12.1 ppbv/h). InVOCs can react with OH and produce peroxyl radicals (HO_2·and RO_2·), consuming

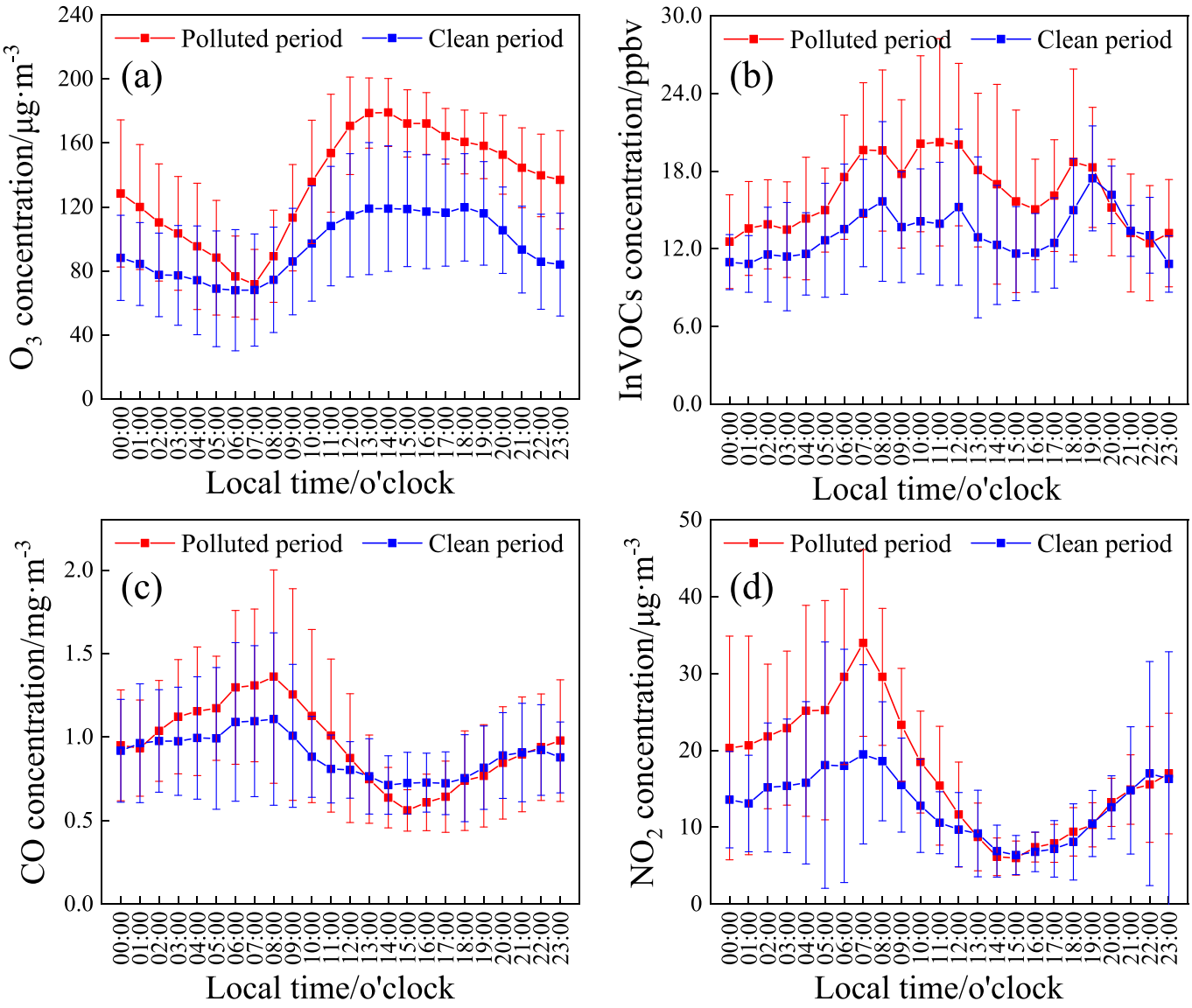

Fig. 2. Diurnal variations in concentrations of atmospheric pollutants during polluted period and clean period ((a), (b), (c) and (d) were O_3, InVOCs, CO and NO_2, respectively).

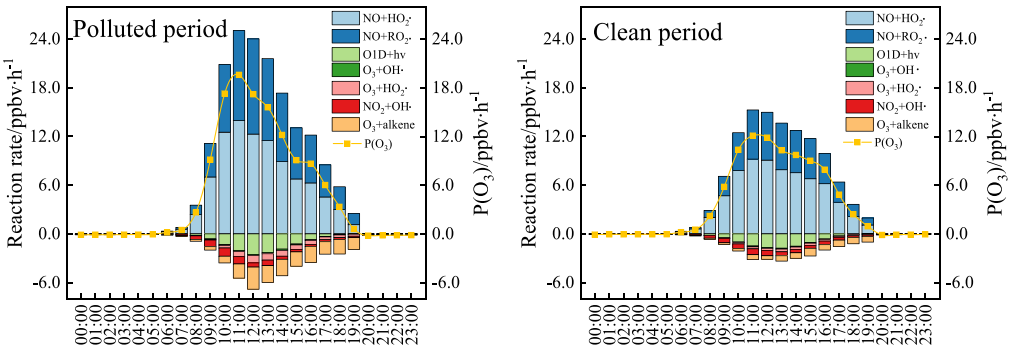

Fig. 3. Diurnal patterns of O_3 production and loss rates simulated by F0AM.

NO and finally causing net O_3 formation (Wang et al., 2023). The O_3 production path was dominated by NO+HO_2·, and the maximum O_3 production rates through NO+HO_2· reached 13.9 ppbv•h^{-1} and 9.2 ppbv•h^{-1} during the polluted period and clean period, respectively. NO+RO_2· was another important O_3 production pathway, and CH_3O_2· + NO was the main reaction pathway. The O_3 loss path mainly included O^1D + hv, O_3 + OH, O_3 + HO_2·, NO_2 + OH and O_3 + alkene. O_3 + alkene was the dominant loss path, accounting for 42.2 % of the total loss path during the polluted period. Compared with other cities, the maximum net (O_3) in Changzhi (16.6 ppbv•h^{-1}) was higher than most cities,such

as Beijing (approximately 13 ppbv•h^{-1}) (Jia et al., 2023), Chengdu (approximately 9 ppbv•h^{-1}) (Liu et al., 2021), Wuhan (approximately 14 ppbv•h^{-1}) (Liu et al., 2021), Hong Kong (approximately 8 ppbv•h^{-1}) (Liu et al., 2019) and the background site in China (approximately 7 ppbv•h^{-1}) (Li et al., 2021a). The higher net (O_3) may be related to the large emission of NO and the higher concentration of HO_2· (as shown in 3.2.2), which indicated that the control of NO is the focus of O_3 reduction in industrial cities.

3.2.2. Diurnal variation and budget analysis of free radical

The free radical concentrations (OH·, HO_2· and H_2O_2) were simulated by the F0AM model in this study (Fig. 4). During the polluted period, the average concentrations of OH·, HO_2· and H_2O_2 were 2.4 × 10^6 molecules•cm^{-3}, 4.0 × 10^8 molecules•cm^{-3} and 0.2 ppbv, respectively, which were 2.1 %, 36.6 % and 36.6 % higher than of those during the clean period, respectively. The concentrations of free radical presented single peak diurnal variation characteristics, and the peak concentrations of OH·, HO_2· and H_2O_2 were 7.4 × 10^6 molecules•cm^{-3} and 9.2 × 10^8 molecules•cm^{-3} and 0.5 ppbv during the whole period, respectively. The peak concentrations of OH· in this study were much higher than Wuhan (6.4 × 10^6 molecules•cm^{-3}), Lanzhou (4.5 × 10^6 molecules•cm^{-3}) and Beijing (2.7 × 10^6 molecules•cm^{-3}) but much lower than the Yangtze River Delta (~9 × 10^6 molecules•cm^{-3}) (Guo, 2022; Slater et al., 2020; Zhang et al., 2021; Zhu et al., 2020). The HO_2· concentrations in this study were higher than those in most regions in China, such as Wuhan (4.7 × 10^8 molecules•cm^{-3}), Beijing (7.3 × 10^8) and the Yangtze River Delta (6.2 × 10^8) (Guo, 2022; Zhu et al., 2020; Jia et al., 2023). OH· are the core of atmospheric chemistry and are an important atmospheric oxidant that can promote the degradation of natural and man-made trace gases (Xue et al., 2016). Thus, the higher OH· concentrations in this study indicated higher atmospheric oxidation. HO_2· is an important free radical reacting with NO and producing O_3, and higher HO_2 concentrations may be the cause of O_3 pollution.

3.2.3. Free radical cycle

The budget of OH-HO_2-RO-RO_2 radicals in the daytime (7 o'clock-19 o'clock) was analyzed to compare the atmospheric photochemical reaction process between the polluted period and clean period (Fig. 5). Evidently, the production of OH· was dominated by the reaction of NO+HO_2· in RO_X· recycling, and the reaction rate during the polluted period (6.9 ppbv•h^{-1}) was 29.0 % higher than that during the clean period (4.9 ppbv•h^{-1}), which was also the main path of O_3 production. The terminated processing of OH was dominated by reactions with NO_2 and NO forming HNO_3 and HONO. The production of HO_2· was dominated by RO· + O_2 (4.9 ppbv•h^{-1} during polluted period) and OH· + CO (1.8 ppbv•h^{-1} during polluted period). The terminated processing of HO_2· was dominated by reactions with HO_2· and RO_2·, forming H_2O_2 and ROOH, respectively. In RO_X· recycling, OH· + VOCs were the main production path of RO_2· (6.1 ppbv•h^{-1} and 3.5 ppbv•h^{-1} during polluted and clean period, respectively) and RO_2· was consumed to form RO· mainly by reacting with NO. RO_2· + NO is also another important path for O_3 generation, and its reaction rate in the polluted period is 43.9 % higher than that in the clean period. HO_2· + NO, RO_2· + NO_2, OH· + VOCs and NO+RO_2· were important reactions of atmospheric photochemical in ROx· recycling, which were significantly higher than those in Shanghai, Chengdu, Hong Kong and were close to the free radical reaction in Zhengzhou and Beijing (Lu et al., 2023a, 2023b; Wang et al., 2022a; Ma et al., 2022; Liu et al., 2019). These reactions are mainly dominated by the O_3 precursors of NO, NO_2 and VOCs (alkene), which are mainly discharged from coal combustion and industrial processes caused by developed industries. The results demonstrated the important role of O_3 precursors in increasing the free radical cycle reaction, which is the basic cause of O_3 pollution and strong atmospheric oxidation.

3.3. O_3 source apportionment

3.3.1. Sensitivity analysis of O_3 formation

The daytime (7 o'clock-19 o'clock) RIR values of O_3 precursors during the polluted period and clean period were analyzed in this study. In total, the decrease in O_3 precursors all led to positive RIR values during the study period, and NOx had the largest sensitivity to the formation of O_3 (RIR = 0.56), followed by InVOCs (RIR = 0.39) and CO (RIR = 0.09). The most sensitive precursor to O_3 varied with different pollution periods. During the polluted period, NOx had the largest RIR value (0.64), followed by InVOCs (0.35) and CO (0.08). During the clean period, InVOCs had the largest RIR value (0.47), followed by NOx (0.41) and CO (0.12). For VOC species, alkenes had the largest RIR value compared to other species, with values of 0.32 and 0.41 during the polluted period and clean period, respectively. Therefore, the results suggested that O_3 precursor control should target alkenes and NOx for a more effective reduction in O_3 pollution. Different from other studies, the sensitivity of NOx in this study was higher than that in Shanghai (approximately −0.1) (Meng et al., 2023), Zibo (approximately −0.4–0.4) (Zheng et al., 2023), and Nanjing (−0.1–0.4) (Wang et al., 2020), suggesting the important role of NOx in O_3 generation in Changzhi.

As shown in Fig. 6, the RIR values of InVOCs (including alkane, alkene, aromatics and alkyne) and NOx exhibited obvious diurnal variation characteristics. During 7 o'clock-9 o'clock, the formation of O_3 was sensitive to InVOCs, but the RIR value of NOx was negative, which was caused by the titration of NOx to O_3 (Liu et al., 2022). Starting from 10 o'clock, the formation of O_3 was controlled by both VOC and NOx. Over time, the RIR of NOx gradually increased and was significantly higher than that of InVOCs, which was more pronounced during polluted periods. At 19 o'clock, the RIR of NOx increased to 1.74 and 1.00 during polluted and clean period, respectively. This RIR analysis result indicated the importance of phased control of O_3 precursors, particularly emphasizing the crucial role of NOx in the O_3 formation process in industrial cities. However, the source of NOx in industrial

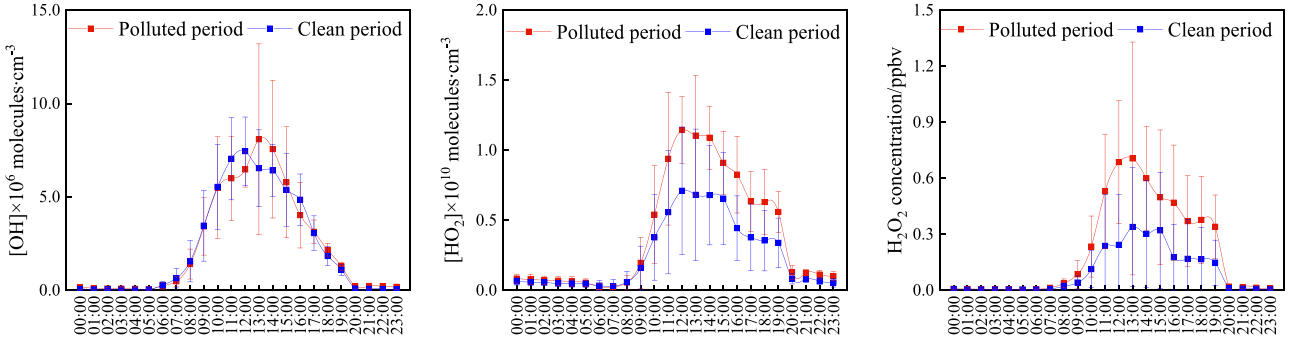

Fig. 4. Diurnal variations of free radical during the polluted period and clean period.

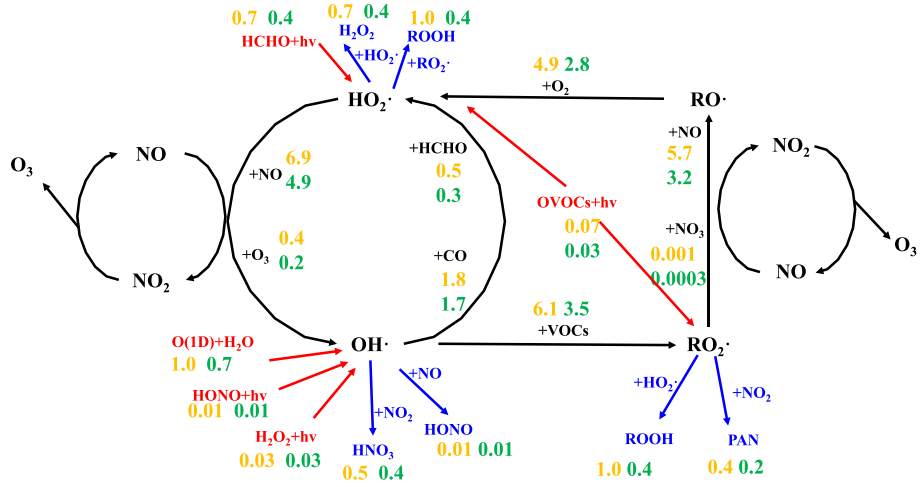

Fig. 5. Summary of daytime average budgets of ROx· (ppbv•h^{-1}). Primary ROx· sources and sinks are in red and blue, respectively. The black lines represent the processes in ROx· recycle. The yellow and green fonts represent the reaction rates during polluted and clean days, respectively.

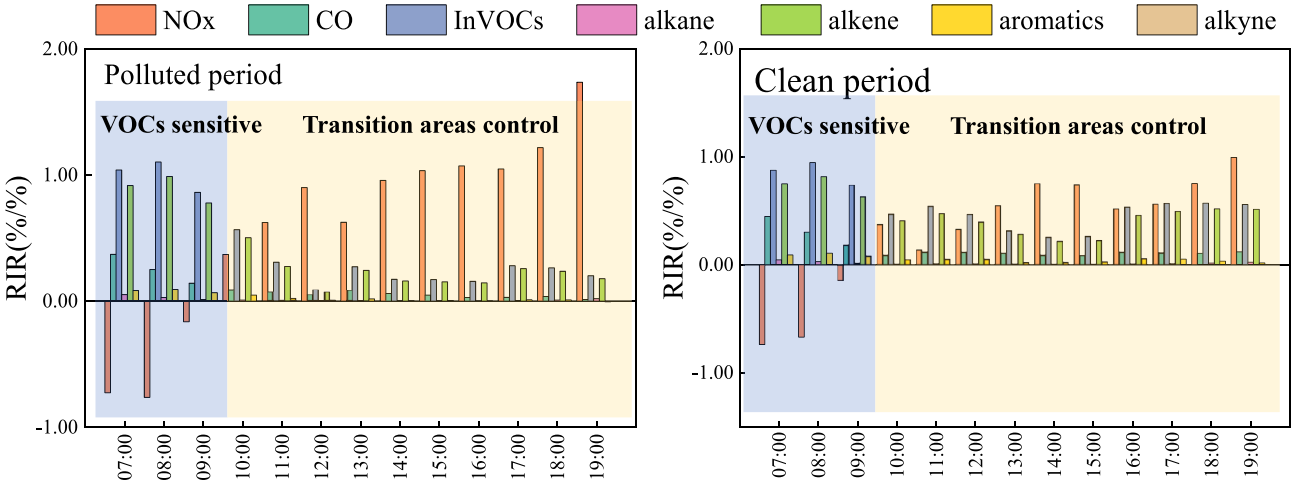

Fig. 6. The daytime RIR values of O_3 precursors (NOx, CO, InVOCs, alkane, alkene, aromatics and alkyne).

cities is complex. In addition to vehicles and coal combustion emissions, heavy industry, represented by coking, steel, cement and other industries, emits large amounts of NOx (Cao et al., 2022; Liu et al., 2018). Therefore, the prevention and control of NOx pollution in industrial cities is particularly important. Industrial cities are typical city transition areas (areas where O_3 is sensitive to VOCs and NOx simultaneously), and the importance of VOCs and NOx should be considered simultaneously in the control process of O_3 pollution in transition areas.

3.3.2. *VOCs source apportionment*

In this study, the PMF 5.0 model was used to analyze the O_3 precursor sources and their contributions. Forty-one InVOC species and NOx were selected for the PMF model. The six factors were identified as industrial process, biogenic source, coal combustion, solvent utilization, diesel vehicle emission and gasoline vehicle emission. The details of the identified sources are shown in Text S2 and Fig. S3.

Fig. 7 shows the source contributions of the six identified factors for InVOCs and NOx. Throughout the study period, gasoline vehicle emissions were the major contributor to InVOCs (27.0 %), followed by coal combustion (20.3 %), diesel vehicle emissions (15.9 %), industrial processes (15.1 %), solvent utilization (14.0 %) and biogenic sources (7.6 %). The contributions of gasoline vehicle emissions, industrial processes, diesel vehicle emissions and biogenic sources to InVOCs during the polluted period (28.4 %, 16.3 %, 16.2 % and 9.9 %) were much higher than those during the clean period (25.0 %, 13.2 %, 15.1 % and 4.6 %). For NOx, coal combustion (44.0 %) and diesel vehicle emissions (35.2 %) had the largest contribution, followed by industrial processes (12.5 %) and gasoline vehicle emissions (8.3 %). Except for coal combustion, other sources all had higher contributions to NOx during the polluted period. In summary, coal combustion and diesel vehicle emissions contribute more to O_3 precursors, which may be attributed to the increase in energy consumption and product transportation caused by developed industries. As a typical industrial city, the production of steel and coke in Changzhi was 6.1 million tons and 15.9 million tons in 2021, respectively, and the production is at a higher level in Shanxi Province (SBS, 2022). One study showed that the steel and coking industries are energy-consuming industries in China and have a significant influence on environmental precursors and O_3 pollution (Wang et al., 2022c). Thus, to control O_3 precursors, industrial cities should pay attention to industrial emission control, especially heavy industry (steel, coking, cement, chemical and so on).

3.3.3. *O_3 source apportionment*

Considering the sensitivity of O_3 to both VOCs and NOx, industrial processes were the main contributor to O_3 (36.7 %), followed by biogenic sources (24.6 %) and coal combustion (18.4 %) throughout the whole study period (Fig. 8). The contributions of industrial processes, biogenic sources, and coal combustion during the polluted period (38.9

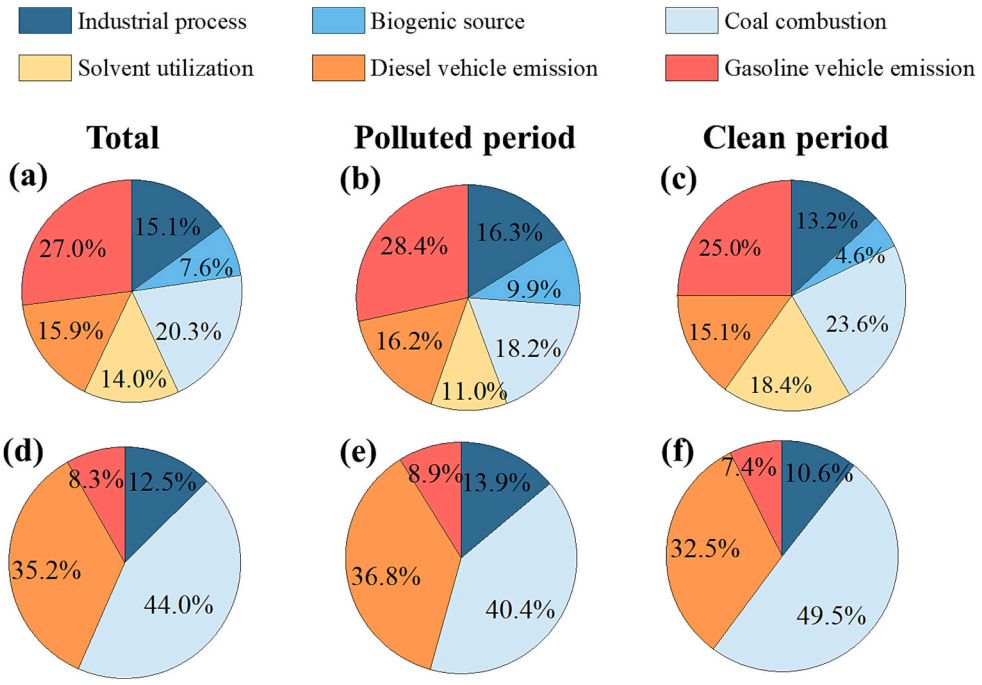

Fig. 7. Source contribution of InVOCs (a, b and c) and NOx (d, e and f) from the PMF model.

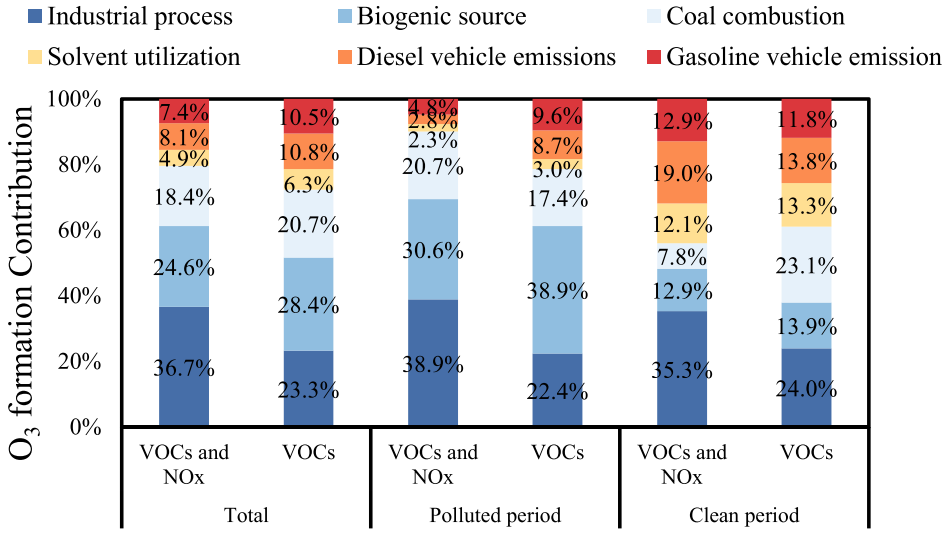

Fig. 8. Source contribution of O_3 simulated by PMF and F0AM.

%, 30.6 % and 20.7 %, respectively) were higher than those during the clean period (35.3 %, 12.9 % and 7.8 %, respectively). Industrial process sources had a significant impact on O_3 (although their contribution to InVOCs is relatively smaller), which was related to their inclusion of highly active VOC species, such as isoprene, 1-hexene, propylene, trans-2-butene, 1-butene, gis-2-butene, trans-2-pentene, 1-pentene, and gis-2-pentene (Wu and Xie, 2017). These highly active VOC species are more likely to promote photochemical reactions and have a greater effect on the generation of O_3 under the action of high temperature during polluted periods (Jia et al., 2023). In addition, coal combustion and biogenic source also contributed greatly to O_3 generation in Changzhi, which may be related to the higher contribution of NOx and VOCs. The concentrations of active VOC species (such as ethene and propylene) in combustion were much higher than those of other sources. Therefore, emission sources containing more highly active VOC species and high concentrations of NOx have a relatively important influence on the generation of O_3. For industrial cities, industrial processes and coal combustion are the focus of control of O_3 and its precursors.

As shown in Fig. 8, considering only the sensitivity of VOCs to O_3, biogenic sources were the main contributor to O_3 (28.4 %), followed by industrial process (23.3 %) and coal combustion (20.7 %). Compared with the results considering the sensitivity of both VOCs and NO_X, this scenario underestimated the contribution of industrial processes and overestimated the contribution of biogenic sources. In addition, the differences between the contributions simulated from the two scenarios were more obvious during the polluted period. Therefore, considering only VOCs and ignoring NOx in the process of source analysis will lead to inaccurate analysis of O_3 sources, which may lead to the incorrect formulation of prevention and control policies. The results emphasize the importance of NO_x in the O_3 formation and source analysis.

3.4. Implication

China has developed heavy industry. In 2021, the production of raw coal, coke, cement and pig iron was 4.1 billion tons, 464.5 million tons, 237.7 million tons and 868.6 million tons, respectively (NBS, 2022). In addition, power generation is still dominated by thermal power, accounting for 68.0 % of the total power generation, which had larger coal consumption. Like Changzhi, there are many industrial cities in China, which result in large and complex emissions of VOCs and NOx. In industrial cities, the steel and coking industries are energy-consuming industries in China and have a significant influence on environmental VOCs and NOx (Wang et al., 2022c). The precursors can increase atmospheric oxidation and speed up the free radical cycle reaction rate, resulting in serious O_3 pollution in industrial cities. Industrial processes and coal combustion are the focus of O_3 control in industrial cities. These sources contain more highly active VOC species (butene, pentene, etc.) and high concentrations of NOx, which have significant importance for O_3 control.

Due to the complex linear relationship between O_3 and precursors, the source analysis of O_3 is complicated, especially for cities with large and complex precursor emissions. Previous studies only considered the influence of VOCs on O_3 generation when analyzing the source of O_3, but this study indicated that the influence of NOx in industrial cities on O_3 generation should not be ignored. Meanwhile, considering only VOCs but not NOx in the analysis of O_3 sources will underestimate the emission proportion of anthropogenic sources (such as coal combustion and industrial processes) and overestimate the proportion of biogenic sources, resulting in inaccurate results. Industrial cities are typical cities in transition areas, and the sensitivity of O_3 to both VOCs and NOx should also be taken into account when analyzing the source of O_3 in transition areas, which can ensure the accuracy of source analysis results. In addition, emission reduction of VOCs and NOx simultaneously should be considered in the control of O_3 in transition areas. This study provides an improved direction for the source analysis of O_3 in industrial cities and even cities in transition areas.

4. Conclusion

This study used F0AM with MCM v3.3.1 to analyze O_3 sensitivities to VOCs and NOx in a typical industrial city in China. The F0AM model results were coupled with a receptor model to analyze the sources of O_3.

Higher concentrations of O_3 precursors were observed during polluted periods indicating that precursor accumulation contributed to the higher max net (O_3) (16.6 ppbv•h^{-1}) and HOx· concentrations. The important reactions in ROx· recycling were mainly dominated by the precursors of NO, NO_2 and alkene, which were mainly discharged from sources caused by the developed industry. This RIR analysis result indicated the importance of phased control of O_3 precursors, particularly emphasizing the crucial role of NOx in the O_3 formation process in industrial cities. Results from PMF analysis indicated that gasoline vehicle emissions, industrial processes, and coal combustion were major sources of O_3 precursors. While industrial process (36.7 %) and biogenic source (24.6 %) were the major sources of O_3. This study highlights the importance of accounting for both VOC and NOx sensitivities when O_3 chemistry is in a transition regime in O_3 production attribution studies.

CRediT authorship contribution statement

Yueyuan Niu: Writing – original draft, Methodology, Investigation, Data curation. **Yulong Yan:** Writing – review & editing, Validation, Supervision, Project administration, Methodology, Conceptualization. **Yiran Xing:** Investigation, Data curation. **Xiaolin Duan:** Investigation, Data curation. **Ke Yue:** Investigation, Data curation. **Jiaqi Dong:** Investigation, Data curation. **Dongmei Hu:** Validation, Methodology. **Yuhang Wang:** Validation, Methodology. **Lin Peng:** Validation, Supervision, Project administration, Conceptualization.

Declaration of competing interest

The authors declare that they have no known competing financial interests or personal relationships that could have appeared to influence the work reported in this paper.

Data availability

Data will be made available on request.

Acknowledgments

This work was supported by the National Natural Science Foundation of China (NSFC) (Grant No. 42330606, No. 21976053, No. 42103056, No. 42273058) and Key Project of Heavy Air Pollution Cause and Control (Grant No. DQGG202108).

Appendix A. Supplementary data

Supplementary data to this article can be found online at https://doi.org/10.1016/j.scitotenv.2024.170559.

References

Atkinson, R., 2003. Kinetics of the gas-phase reactions of oh radicals with alkanes and cycloalkanes. Atmos. Chem. Phys. 3 (6), 2233–2307. https://doi.org/10.5194/acp-3-2233-2003.

Atkinson, R., Arey, J., 2003. Atmospheric degradation of volatile organic compounds. Chem. Rev. 103 (12), 4605–4638. https://doi.org/10.1021/cr0206420.

Cao, J., Liu, C., Qiu, X., Peng, L., 2022. Research on high-resolution emission inventory of air pollution sources in Changzhi. Environ. Pollut. Cont. 44 (5), 618–624. https://doi.org/10.15985/j.cnki.1001-3865.2022.05.012.

Cardelino, C.A., Chameides, W.L., 1995. An observation-based model for analyzing ozone precursor relationships in the urban atmosphere. J. Air Waste Manag. Assoc. 45 (3), 161–180. https://doi.org/10.1080/10473289.1995.10467356.

CNEMC. China National Environmental Centre, http://www.cnemc.cn/, last access: 1 January 2023.

Cohen, A.J., Brauer, M., Burnett, R., Anderson, H.R., Frostad, J., Estep, K., Balakrishnan, K., Brunekreef, B., Dandona, L., Dandona, R., Feigin, V., Freedman, G., Hubbell, B., Jobling, A., Kan, H., Knibbs, L., Liu, Y., Martin, R., Morawska, L., Pope, C.R., Shin, H., Straif, K., Shaddick, G., Thomas, M., van Dingenen, R., van Donkelaar, A., Vos, T., Murray, C., Forouzanfar, M.H., 2017. Estimates and 25-year trends of the global burden of disease attributable to ambient air pollution: an analysis of data from the global burden of diseases study 2015. Lancet 389 (10082), 1907–1918. https://doi.org/10.1016/S0140-6736(17)30505-6.

Ding, J., Dai, Q., Fan, W., Lu, M., Zhang, Y., Han, S., Feng, Y., 2023. Impacts of meteorology and precursor emission change on O_3 variation in Tianjin, China from 2015 to 2021. J. Environ. Sci. 126, 506–516. https://doi.org/10.1016/j.jes.2022.03.010.

Duan, X., Yan, Y., Li, R., Deng, M., Hu, D., Peng, L., 2021. Seasonal variations, source apportionment, and health risk assessment of trace metals in $PM_{2.5}$ in the typical industrial city of Changzhi, China. Atmos. Pollut. Res. 12 (1), 365–374. https://doi.org/10.1016/j.apr.2020.09.017.

Fan, M., Zhang, Y., Lin, Y., Li, L., Xie, F., Hu, J., Mozaffar, A., Cao, F., 2021. Source apportionments of atmospheric volatile organic compounds in Nanjing, China during high ozone pollution season. Chemosphere 263, 128025. https://doi.org/10.1016/j.chemosphere.2020.128025.

Gao, Q., Yan, Y., Li, R., Xu, Y., Niu, Y., Liu, C., Xie, K., Chang, Z., Hu, D., Li, Z., Peng, L., 2020. Characteristics of volatile organic compounds during different pollution periods in winter in Yuncheng, a typical city in North China. Aerosol Air Qual. Res. 20 (1), 97–107. https://doi.org/10.4209/aaqr.2019.08.0402.

Guo, W., 2022. Ozone Pollution Characteristics, Formation Mechanism, and Prevention Strategies in a Valley Petrochemical Industrial City, Northwestern China. Ph.D. thesis,. School of atmospheric Sciences, Lanzhou University, China.

Guo, W., Yang, Y., Chen, Q., Zhu, Y., Zhang, Y., Zhang, Y., Liu, Y., Li, G., Sun, W., She, J., 2022. Chemical reactivity of volatile organic compounds and their effects on ozone formation in a petrochemical industrial area of Lanzhou, western China. Sci. Total Environ. 839, 155901 https://doi.org/10.1016/j.scitotenv.2022.155901.

Han, J., Liu, Z., Hu, B., Zhu, W., Tang, G., Liu, Q., Ji, D., Wang, Y., 2023. Observations and explicit modeling of summer and autumn ozone formation in urban Beijing: identification of key precursor species and sources. Atmos. Environ. 309, 119932 https://doi.org/10.1016/j.atmosenv.2023.119932.

Hui, L., Liu, X., Tan, Q., Feng, M., An, J., Qu, Y., Zhang, Y., Jiang, M., 2018. Characteristics, source apportionment and contribution of VOCs to ozone formation in Wuhan, Central China. Atmos. Environ. 192, 55–71. https://doi.org/10.1016/j.atmosenv.2018.08.042.

Jia, C., Tong, S., Zhang, X., Li, F., Zhang, W., Li, W., Wang, Z., Zhang, G., Tang, G., Liu, Z., Ge, M., 2023. Atmospheric oxidizing capacity in autumn Beijing: analysis of

the O_3 and $PM_{2.5}$ episodes based on observation-based model. J. Environ. Sci. (China) 124, 557–569. https://doi.org/10.1016/j.jes.2021.11.020.
Li, J., Hao, Y., Simayi, M., Shi, Y., Xi, Z., Xie, S., 2019. Verification of anthropogenic VOC emission inventory through ambient measurements and satellite retrievals. Atmos. Chem. Phys. 19 (9), 5905–5921. https://doi.org/10.5194/acp-19-5905-2019.
Li, R., Yan, Y., Peng, L., Wang, F., Lu, X., Wang, Y., Xu, Y., Wang, C., 2021. Enhancement of ozone formation by increased vehicles emission and reduced coal combustion emission in Taiyuan, a traditional industrial city in northern China. Atmos. Environ. 267, 118759 https://doi.org/10.1016/j.atmosenv.2021.118759.
Li, Y., Gao, R., Xue, L., Wu, Z., Yang, X., Gao, J., Ren, L., Li, H., Ren, Y., Li, G., Li, C., Yan, Z., Hu, M., Zhang, Q., Xu, Y., 2021a. Ambient volatile organic compounds at Wudang mountain in Central China: characteristics, sources and implications to ozone formation. Atmos. Res. 250, 105359 https://doi.org/10.1016/j.atmosres.2020.105359.
Liu, H., Wu, B., Liu, S., Shao, P., Liu, X., Zhu, C., Wang, Y., Wu, Y., Xue, Y., Gao, J., Hao, Y., Tian, H., 2018. A regional high-resolution emission inventory of primary air pollutants in 2012 for Beijing and the surrounding five provinces of North China. Atmos. Environ. 181, 20–33. https://doi.org/10.1016/j.atmosenv.2018.03.013.
Liu, P., Xue, C., Ye, C., Liu, C., Zhang, C., Wang, J., Zhang, Y., Liu, J., Mu, Y., 2022. The lack of HONO measurement may affect the accurate diagnosis of ozone production sensitivity. ACS Environ. Au. https://doi.org/10.1021/acsenvironau.2c00048.
Liu, X., Lyu, X., Wang, Y., Jiang, F., Guo, H., 2019. Intercomparison of O_3 formation and radical chemistry in the past decade at a suburban site in Hong Kong. Atmos. Chem. Phys. 19 (7), 5127–5145. https://doi.org/10.5194/acp-19-5127-2019.
Liu, X., Guo, H., Zeng, L., Lyu, X., Wang, Y., Zeren, Y., Yang, J., Zhang, L., Zhao, S., Li, J., Zhang, G., 2021. Photochemical ozone pollution in five Chinese megacities in summer 2018. Sci. Total Environ. 801, 149603 https://doi.org/10.1016/j.scitotenv.2021.149603.
Lu, B., Zhang, Z., Jiang, J., Meng, X., Liu, C., Herrmann, H., Chen, J., Xue, L., Li, X., 2023a. Unraveling the O_3-NOx-VOCs relationships induced by anomalous ozone in industrial regions during COVID-19 in Shanghai. Atmos. Environ. 308, 119864 https://doi.org/10.1016/j.atmosenv.2023.119864.
Lu, B., Zhang, Z., Jiang, J., Meng, X., Liu, C., Herrmann, H., Chen, J., Xue, L., Li, X., 2023b. Unraveling the O_3-NOx-VOCs relationships induced by anomalous ozone in industrial regions during COVID-19 in Shanghai. Atmos. Environ. 308, 119864 https://doi.org/10.1016/j.atmosenv.2023.119864.
Lu, K., Zhang, Y., Su, H., Brauers, T., Chou, C.C., Hofzumahaus, A., Liu, S.C., Kita, K., Kondo, Y., Shao, M., Wahner, A., Wang, J., Wang, X., Zhu, T., 2010. Oxidant (O_3+NO_2) production processes and formation regimes in Beijing. J. Geophys. Res. 115 (D7) https://doi.org/10.1029/2009JD012714.
Ma, W., Feng, Z., Zhan, J., Liu, Y., Liu, P., Liu, C., Ma, Q., Yang, K., Wang, Y., He, H., Kulmala, M., Mu, Y., Liu, J., 2022. Influence of photochemical loss of volatile organic compounds on understanding ozone formation mechanism. Atmos. Chem. Phys. 22 (7), 4841–4851. https://doi.org/10.5194/acp-22-4841-2022.
Meng, X., Jiang, J., Chen, T., Zhang, Z., Lu, B., Liu, C., Xue, L., Chen, J., Herrmann, H., Li, X., 2023. Chemical drivers of ozone change in extreme temperatures in eastern China. Sci. Total Environ. 874, 162424 https://doi.org/10.1016/j.scitotenv.2023.162424.
MEP. Ministry of Ecology and Environment of the People's Republic of China, https://www.mee.gov.cn/hjzl/sthjzk/zghjzkgb/, last access: 1 November 2022.
Mozaffar, A., Zhang, Y., Lin, Y., Xie, F., Fan, M., Cao, F., 2021. Measurement report: high contributions of halocarbon and aromatic compounds to atmospheric volatile organic compounds in an industrial area. Atmos. Chem. Phys. 21 (23), 18087–18099. https://doi.org/10.5194/acp-21-18087-2021.
NBS. National Bureau of Statistics, http://www.stats.gov.cn/sj/, last access: 1 December 2022.
Ninneman, M., Jaffe, D.A., 2021. The impact of wildfire smoke on ozone production in an urban area: insights from field observations and photochemical box modeling. Atmos. Environ. 267, 118764 https://doi.org/10.1016/j.atmosenv.2021.118764.
Niu, Y., Yan, Y., Chai, J., Zhang, X., Xu, Y., Duan, X., Wu, J., Peng, L., 2022. Effects of regional transport from different potential pollution areas on volatile organic compounds (VOCs) in northern Beijing during non-heating and heating periods. Sci. Total Environ. 836, 155465 https://doi.org/10.1016/j.scitotenv.2022.155465.
Norris, G., Duvall, R., Brown, S., Bai, S., 2014. EPA Positive Matrix Factorization (PMF) 5.0. Fundamentals and User Guide, Washington, DC (EPA/600/R-14/108 (NTISPB2015-105147).
SBS. Shanxi provincial Bureau of Statistics, https://tjj.shanxi.gov.cn/, last access: 1 December 2022.
Simayi, M., Shi, Y., Xi, Z., Ren, J., Hini, G., Xie, S., 2022. Emission trends of industrial VOCs in China since the clean air action and future reduction perspectives. Sci. Total Environ. 826, 153994.
Slater, E.J., Whalley, L.K., Woodward-Massey, R., Ye, C., Lee, J.D., Squires, F., Hopkins, J.R., Dunmore, R.E., Shaw, M., Hamilton, J.F., Lewis, A.C., Crilley, L.R., Kramer, L., Bloss, W., Vu, T., Sun, Y., Xu, W., Yue, S., Ren, L., Acton, W.J.F., Hewitt, C.N., Wang, X., Fu, P., Heard, D.E., 2020. Elevated levels of oh observed in haze events during wintertime in Central Beijing. Atmos. Chem. Phys. 20 (23), 14847–14871. https://doi.org/10.5194/acp-20-14847-2020.
Sommariva, R., Cox, S., Martin, C., Borońska, K., Young, J., Jimack, P.K., Pilling, M.J., Matthaios, V.N., Nelson, B.S., Newland, M.J., Panagi, M., Bloss, W.J., Monks, P.S., Rickard, A.R., 2020. Atchem (version 1), an open-source box model for the master chemical mechanism. Geosci. Model Dev. 13 (1), 169–183. https://doi.org/10.5194/gmd-13-169-2020.
Tan, Q., Ge, B., Xu, X., Gan, L., Yang, W., Chen, X., Pan, X., Wang, W., Li, J., Wang, Z., 2022. Increasing impacts of the relative contributions of regional transport on air pollution in Beijing: observational evidence. Environ. Pollut. 292, 118407 https://doi.org/10.1016/j.envpol.2021.118407.
Tan, Z., Lu, K., Jiang, M., Su, R., Wang, H., Lou, S., Fu, Q., Zhai, C., Tan, Q., Yue, D., Chen, D., Wang, Z., Xie, S., Zeng, L., Zhang, Y., 2019. Daytime atmospheric oxidation capacity in four Chinese megacities during the photochemically polluted season: a case study based on box model simulation. Atmos. Chem. Phys. 6 (19), 3493–3513.
Wang, H., Sun, Y., Wang, F., Wei, W., Zhao, Z., Zhang, J., Lin, X., Ma, S., 2021. Characteristics, ozone formation potential and source apportionment of VOCs during epidemic prevention in Jiyuan. Acta Sci. Circumst. 41 (03), 761–769.
Wang, J., Zhang, Y., Wu, Z., Luo, S., Song, W., Wang, X., 2022. Ozone episodes during and after the 2018 Chinese national day holidays in Guangzhou: implications for the control of precursor VOCs. J. Environ. Sci. (China) 114, 322–333. https://doi.org/10.1016/j.jes.2021.09.009.
Wang, M., Chen, W., Zhang, L., Qin, W., Zhang, Y., Zhang, X., Xie, X., 2020. Ozone pollution characteristics and sensitivity analysis using an observation-based model in Nanjing, Yangtze River Delta region of China. J. Environ. Sci. (China) 93, 13–22. https://doi.org/10.1016/j.jes.2020.02.027.
Wang, R., Wang, X., Cheng, S., Wang, K., Cheng, L., Zhu, J., Zheng, H., Duan, W., 2022c. Emission characteristics and reactivity of volatile organic compounds from typical high-energy-consuming industries in North China. Sci. Total Environ. 809, 151134 https://doi.org/10.1016/j.scitotenv.2021.151134.
Wang, R., Wang, L., Xue, M., Chen, N., Zhang, L., Ling, Z., Li, T., Tao, M., Wang, Y., 2023. New insight into formation mechanism, source and control strategy of severe O_3 pollution: the case from photochemical simulation in the Wuhan metropolitan area, Central China. Atmos. Res. 284, 106605 https://doi.org/10.1016/j.atmosres.2023.106605.
Wang, T., Xue, L., Brimblecombe, P., Lam, Y.F., Li, L., Zhang, L., 2017. Ozone pollution in China: a review of concentrations, meteorological influences, chemical precursors, and effects. Sci. Total Environ. 575, 1582–1596. https://doi.org/10.1016/j.scitotenv.2016.10.081.
Wang, X., Yin, S., Zhang, R., Yuan, M., Ying, Q., 2022a. Assessment of summertime O_3 formation and the O_3-NO_x-VOC sensitivity in Zhengzhou, China using an observation-based model. Sci. Total Environ. 813, 152449 https://doi.org/10.1016/j.scitotenv.2021.152449.
Wang, Z., Shi, Z., Wang, F., Liang, W., Shi, G., Wang, W., Chen, D., Liang, D., Feng, Y., Russell Armistead, G., 2022b. Implications for ozone control by understanding the survivor bias in observed ozone-volatile organic compounds system. NPJ Clim. Atmos. Sci. 5 (1), 1–9. https://doi.org/10.1038/s41612-022-00261-7.
Wolfe, G.M., Marvin, M.R., Roberts, S.J., Travis, K.R., Liao, J., 2016. The framework for 0-D atmospheric modeling (F0AM) v3.1. Geosci. Model Dev. 9 (9), 3309–3319. https://doi.org/10.5194/gmd-9-3309-2016.
Wu, R., Xie, S., 2017. Spatial distribution of ozone formation in China derived from emissions of speciated volatile organic compounds. Environ. Sci. Technol. 51 (5), 2574–2583. https://doi.org/10.1021/acs.est.6b03634.
Xu, Z., Huang, X., Nie, W., Chi, X., Xu, Z., Zheng, L., Sun, P., Ding, A., 2017. Influence of synoptic condition and holiday effects on VOCs and ozone production in the Yangtze River Delta region, China. Atmos. Environ. 168, 112–124. https://doi.org/10.1016/j.atmosenv.2017.08.035.
Xuan, H., Zhao, Y., Ma, Q., Chen, T., Liu, J., Wang, Y., Liu, C., Wang, Y., Liu, Y., Mu, Y., He, H., 2023. Formation mechanisms and atmospheric implications of summertime nitrous acid (HONO) during clean, ozone pollution and double high-level $PM_{2.5}$ and O_3 pollution periods in Beijing. Sci. Total Environ. 857, 159538 https://doi.org/10.1016/j.scitotenv.2022.159538.
Xue, L., Gu, R., Wang, T., Wang, X., Saunders, S., Blake, D., Louie, P.K.K., Luk, C.W.Y., Simpson, I., Xu, Z., Wang, Z., Gao, Y., Lee, S., Mellouki, A., Wang, W., 2016. Oxidative capacity and radical chemistry in the polluted atmosphere of Hongkong and Pearl River Delta region: analysis of a severe photochemical smog episode. Atmos. Chem. Phys. 16 (15), 9891–9903. https://doi.org/10.5194/acp-16-9891-2016.
Yuan, B., Hu, W.W., Shao, M., Wang, M., Chen, W.T., Lu, S.H., Zeng, L.M., Hu, M., 2013. VOC emissions, evolutions and contributions to SOA formation at a receptor site in eastern China. Atmos. Chem. Phys. 13 (17), 8815–8832. https://doi.org/10.5194/acp-13-8815-2013.
Zeng, P., Lyu, X.P., Guo, H., Cheng, H.R., Jiang, F., Pan, W.Z., Wang, Z.W., Liang, S.W., Hu, Y.Q., 2018. Causes of ozone pollution in summer in Wuhan, Central China. Environ. Pollut. 241, 852–861. https://doi.org/10.1016/j.envpol.2018.05.042.
Zhang, K., Huang, L., Li, Q., Huo, J., Duan, Y., Wang, Y., Yaluk, E., Wang, Y., Fu, Q., Li, L., 2021. Explicit modeling of isoprene chemical processing in polluted air masses in suburban areas of the Yangtze River Delta region: radical cycling and formation of ozone and formaldehyde. Atmos. Chem. Phys. 21 (8), 5905–5917. https://doi.org/10.5194/acp-21-5905-2021.
Zhang, K., Liu, Z., Zhang, X., Li, Q., Jensen, A., Tan, W., Huang, L., Wang, Y., de Gouw, J., Li, L., 2022. Insights into the significant increase in ozone during COVID-19 in a typical urban city of China. Atmos. Chem. Phys. 22 (7), 4853–4866. https://doi.org/10.5194/acp-22-4853-2022.
Zhao, M., Zhang, Y., Pei, C., Chen, T., Mu, J., Liu, Y., Wang, Y., Wang, W., Xue, L., 2022. Worsening ozone air pollution with reduced NO and VOCs in the Pearl River Delta region in autumn 2019: implications for national control policy in China. J. Environ. Manag. 324, 116327 https://doi.org/10.1016/j.jenvman.2022.116327.
Zheng, Z., Li, K., Xu, B., Dou, J., Li, L., Zhang, G., Li, S., Geng, C., Yang, W., Azzi, M., Bai, Z., 2023. O_3–precursor relationship over multiple patterns of timescale: a case study in Zibo, Shandong province. China. Atmos. Chem. Phys. 23 (4), 2649–2665. https://doi.org/10.5194/acp-23-2649-2023.
Zhu, J., Cheng, H., Peng, J., Zeng, P., Wang, Z., Lyu, X., Guo, H., 2020. O_3 photochemistry on O_3 episode days and non-O_3 episode days in Wuhan, Central China. Atmos. Environ. 223, 117236 https://doi.org/10.1016/j.atmosenv.2019.117236.